

## Article

# Tetrafluorosubstituted Metal Phthalocyanines: Study of the Effect of the Position of Fluorine Substituents on the Chemiresistive Sensor Response to Ammonia

Darya Klyamer <sup>1,\*</sup>, Dmitry Bonegardt <sup>1</sup>, Pavel Krasnov <sup>2</sup>, Alexander Sukhikh <sup>1</sup>, Pavel Popovetskiy <sup>1</sup> and Tamara Basova <sup>1</sup>

<sup>1</sup> Nikolaev Institute of Inorganic Chemistry SB RAS, 3 Lavrentiev Pr., 630090 Novosibirsk, Russia

<sup>2</sup> International Research Center of Spectroscopy and Quantum Chemistry, Siberian Federal University, 26 Kirensky St., 660074 Krasnoyarsk, Russia

\* Correspondence: klyamer@niic.nsc.ru

**Abstract:** A comparative analysis of the chemiresistive sensor response of thin films of a series of tetrasubstituted phthalocyanines of various metals with F-substituent in peripheral (MPcF<sub>4</sub>-p, M = Cu, Co, Zn, Pb, VO) and non-peripheral (MPcF<sub>4</sub>-np) positions in macroring to low concentrations of ammonia (1–50 ppm) was carried out. It was found that MPcF<sub>4</sub>-p films exhibit a higher sensor response than MPcF<sub>4</sub>-np ones. A CoPcF<sub>4</sub>-p film demonstrated a calculated LOD of 0.01 ppm with a recovery time of 215 s, while a VOPcF<sub>4</sub>-p film had LOD of 0.04 ppm and the recovery time of 270 s. The selectivity test showed that CO<sub>2</sub>, ethanol, acetone, benzene, and formaldehyde did not interfere with the determination of ammonia, while H<sub>2</sub>S at a concentration of more than 10 ppm could act as an interfering gas. It was shown that, as a result of quantum-chemical calculations, the observed regularities are best described by the interaction of NH<sub>3</sub> with phthalocyanines through the formation of hydrogen bonds between NH<sub>3</sub> and side atoms of the macroring. In the case of MPcF<sub>4</sub>-p, the NH<sub>3</sub> molecule approaches the macrocycle more closely and binds more strongly than in the case of MPcF<sub>4</sub>-np. The stronger binding leads to a stronger effect of the ammonia molecule on the electronic structure of phthalocyanine and, as a consequence, on the chemiresistive sensor response of the films to ammonia.

**Keywords:** metal phthalocyanines; fluorine substituents; ammonia; chemiresistive sensors; DFT calculations



**Citation:** Klyamer, D.; Bonegardt, D.; Krasnov, P.; Sukhikh, A.; Popovetskiy, P.; Basova, T. Tetrafluorosubstituted Metal Phthalocyanines: Study of the Effect of the Position of Fluorine Substituents on the Chemiresistive Sensor Response to Ammonia. *Chemosensors* **2022**, *10*, 515. <https://doi.org/10.3390/chemosensors10120515>

Academic Editor: Elisabetta Comini

Received: 6 November 2022

Accepted: 2 December 2022

Published: 4 December 2022

**Publisher's Note:** MDPI stays neutral with regard to jurisdictional claims in published maps and institutional affiliations.



**Copyright:** © 2022 by the authors. Licensee MDPI, Basel, Switzerland. This article is an open access article distributed under the terms and conditions of the Creative Commons Attribution (CC BY) license (<https://creativecommons.org/licenses/by/4.0/>).

## 1. Introduction

Ammonia (NH<sub>3</sub>) is one of the most toxic gases in nature. It has a toxic effect on the human body, an irritating effect on the mucous membranes and skin, and causes pulmonary edema and severe damage to the nervous system [1,2]. Ammonia is one of the main products in the chemical industry; for example, it is widely used in the production of fertilizers, explosives, medicine and agriculture, as well as the production of polymers, nitric acid, and also as a refrigerant [3,4]. Normally, the gas content in the ambient air should not exceed 2 mg/m<sup>3</sup>. The human sense of smell is able to detect the characteristic sharp ammonia smell only at a gas concentration of 37 mg/m<sup>3</sup>, when it poses a direct danger to health and life [5,6]. Therefore, it is important to use gas sensors to monitor the ammonia content in the atmosphere [6,7]. The release of large amounts of NH<sub>3</sub> can lead to serious poisoning. Thus, constant monitoring of the amount of ammonia in enterprises or in the surrounding atmosphere is necessary to prevent environmental disasters. This fact prompted the search for new materials for the rapid, selective, and sensitive detection. At the same time, the sensors must be able to operate at variable humidity and temperature.

In addition to the determination of ammonia in the surrounding atmosphere, one of the important directions where analysis of NH<sub>3</sub> concentrations is required is the non-invasive diagnosis of various diseases by the composition of exhaled air. Conclusions about

changes in metabolism or the presence of a disease can be made by changing the ratio of substances released during exhalation. For example, an ammonia concentration of more than 1 ppm indicates renal insufficiency in nephritis, atherosclerosis of the renal arteries, or toxic kidney lesions [8,9]. The test for the content of ammonia in exhaled air can also be used to monitor hemodialysis in acute or chronic renal failure [10]. Therefore, the search for new materials that are selective with respect to ammonia and sensitive to such low concentrations is also an urgent task.

Several types of gas analyzers are used to control the concentration of ammonia [11]. Among them, electrochemical ammonia sensors have become the most popular due to the best combination of price and reliability of results [12]. The disadvantage of such ammonia sensors is the dependence of their readings on temperature and humidity. Semiconductor ammonia sensors have a low cost, but the main disadvantages of this type of ammonia sensors include selectivity. Therefore, the search for new materials that can act as active layers of sensor devices is constantly underway.

Thin films of metal oxides ( $\text{SnO}_2$ ,  $\text{In}_2\text{O}_3$ ,  $\text{Ga}_2\text{O}_3$ ,  $\text{WO}_3$ ,  $\text{V}_2\text{O}_5$ , etc.) [13,14], carbon nano-materials [15,16], conducting organic polymers [17,18], and metal phthalocyanines [19,20] are most often used as materials of sensitive layers of chemiresistive sensors to detect ammonia. Among these materials, phthalocyanines are distinguished by high sensitivity, exceptional chemical and thermal stability, and the ability to form ordered thin films during deposition by both physical vapor deposition (PVD) [21] and solution methods (e.g., spin coating, Langmuir Blodgett, and drop casting) [22]. The properties of phthalocyanines can be regulated by introducing various central metals and substituents into their aromatic macroring.

In a number of early studies, it was shown that the introduction of electron-acceptor substituents, such as fluorine, led to an increase in the sensitivity of the sensor to electron-donating gases, which include ammonia [21,23,24]. The introduction of fluorine substituents leads to a decrease in the electron density of the aromatic macrocycle and an increase in the oxidative potential of the phthalocyanine molecules [25,26]. Apart from this, the introduction of F-substituents leads to a lower level of LUMO energy, which promotes the injection of electrons and, consequently, affects their semiconductor properties [27,28].

In our previous studies, the chemiresistive sensor response of unsubstituted (MPc) phthalocyanines, tetra- ( $\text{MPcF}_4$ ) and hexadecafluorosubstituted ( $\text{MPcF}_{16}$ ) phthalocyanines of Cu, Zn, and Co to ammonia was studied and it was shown that the sensor response increased in the following order:  $\text{MPc} < \text{MPcF}_{16} < \text{MPcF}_4$ .  $\text{MPcF}_4$  ( $M = \text{Zn}, \text{Co}$ ) layers were shown to demonstrate the best sensor performance, with the calculated detection limit of  $\text{NH}_3$  reaching to 0.01 ppm and an average response time of 15 sec [21]. It has been mentioned that thin films of tetrafluorinated phthalocyanine of other metals (viz. with  $M = \text{Pb}, \text{VO}, \text{Fe}$ ) also exhibited sensor response to ammonia, but the detailed characteristics of the sensors were not investigated. In addition, it is known that in the case of tetrafluorosubstituted MPc substituents can be introduced into both peripheral ( $\text{MPcF}_4\text{-p}$ ) and non-peripheral ( $\text{MPcF}_4\text{-np}$ ) positions of the aromatic ring of phthalocyanine (Figure 1). At the same time, it should be noted that there are only sporadic works on the study of the sensor properties of  $\text{MPcF}_4\text{-np}$  films in the literature [29].

This work is aimed at a comparative analysis of the sensor response of thin films of a series of tetrasubstituted phthalocyanine of various metals with F-substituent in peripheral ( $\text{MPcF}_4\text{-p}$ ,  $M = \text{Cu}, \text{Co}, \text{Zn}, \text{Pb}, \text{VO}$ ) and non-peripheral ( $\text{MPcF}_4\text{-np}$ ) positions in macroring to low concentrations of ammonia (1–50 ppm). The quantum-chemical calculations are performed to study the interaction nature between the phthalocyanine and analyte molecules and to explain the observed regularities. This contributes to a more complete understanding of the relationship between structure and properties, and allows the selection of phthalocyanine films with the most attractive properties (sensitivity, detection limits, response and recovery times) for the development of active layers of chemiresistive gas sensors for the determination of ammonia.

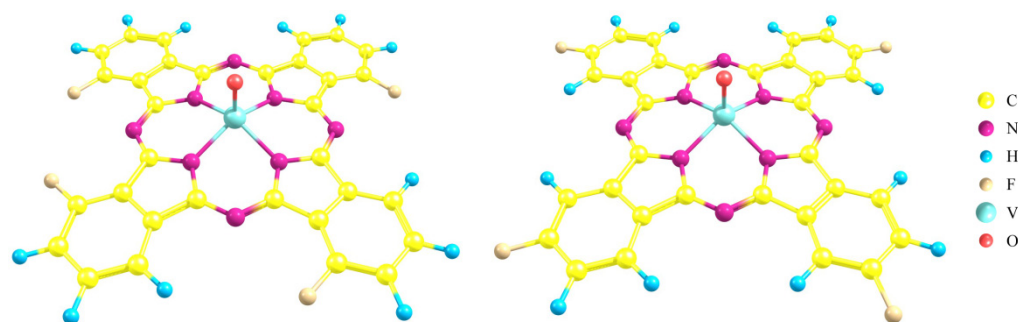


**Figure 1.** Structure of tetrafluorosubstituted metal phthalocyanines with F-substituents in non-peripheral (MPcF<sub>4</sub>-np, **left**) and peripheral (MPcF<sub>4</sub>-p, **right**) positions.

## 2. Materials and Methods

### 2.1. Synthesis of MPcF<sub>4</sub> and Deposition of Their Films

MPcF<sub>4</sub>-p and MPcF<sub>4</sub>-np derivatives were synthesized by the method of template synthesis by fusing a mixture (1:4) of a salt (chloride or acetate) of the corresponding metal with 4-fluorophthalonitrile (Sigma-Aldrich, CAS 65610-14-2) or 3-fluorophthalonitrile (Fluorochem, CAS 65610-13-1), respectively, as was described in our previous works in more detail [30,31]. The prepared MPcF<sub>4</sub>-p and MPcF<sub>4</sub>-np powders were purified by vacuum ( $10^{-5}$  Torr) gradient sublimation; the sublimation temperature was 420–450 °C.

Thin films of the phthalocyanines with a nominal thickness of about 100 nm were deposited by a PVD method in vacuum of  $10^{-5}$  Torr. Glass slides with pre-deposited interdigitated Pt electrodes (IDE, G-IDEPT10, Metrohm, DropSens, Spain) were used as substrates; the substrate temperature was 60 °C. The IDE has the cell constant of  $0.0188 \text{ cm}^{-1}$ , the number of digits of  $125 \times 2$  and the digit length of 6760  $\mu\text{m}$ .

The XRD study of thin films was carried out using a Bruker D8 advance powder diffractometer (vertical  $\theta$ - $\theta$  goniometer in Bragg–Brentano geometry, Cu-anode sealed tube 40 mA at 40 kV, LYNXEYE XE-T compound silicon strip detector, motorized divergence slit in fixed sample illumination area mode) with  $2\theta$  scan step of  $0.01023^\circ$ , and the acquisition time of 2 s/step.

The morphology of the MPcF<sub>4</sub>-p and MPcF<sub>4</sub>-np films was studied by atomic force microscopy (AFM) in the semicontact mode using the Ntegra Prima II nanolaboratory (NT-MDT, Moscow, Russia). The parameters of the HA\_NC probe were as follows: thickness—3  $\mu\text{m}$ , probe length—123  $\mu\text{m}$ , width—34 mm, force constant—17 N/m, resonant frequency—230 kHz. A Nova SPM software (standards ISO 4287-1, ISO 4287, and ASME B46) was used to calculate roughness parameters.

### 2.2. Investigation of the Chemiresistive Sensor Response

Sensor properties of the investigated films were studied by measuring the change in the resistance when exposed to ammonia in a wide range of concentrations (1–100 ppm). The change in the resistance was measured using a Keithley 236 universal electrometer by applying a constant DC voltage (10 V). The normalized sensor response was calculated as  $R_n = (R - R_0)/R_0$ ; where R is the steady resistance of the MPcF<sub>4</sub> film at a certain NH<sub>3</sub> concentration and R<sub>0</sub> is the baseline resistance of the film in air. Three different samples were used to calculate the standard deviation of the values of sensor response. The scheme of the installation for studying sensor properties and a photograph of a flowing gas cell were presented in our previous publication [29].

Pure commercial NH<sub>3</sub> gas (Company “Chistyie Gasy”, Novosibirsk, Russia) was used as an analyte source; air was used as a carrier and diluent gas. The gas flow was regulated using mass flow regulators and passed through the cell at the constant flow rate of  $300 \text{ mL} \cdot \text{min}^{-1}$ .

### 2.3. Quantum-Chemical Calculations

Quantum-chemical calculations of the geometric structure and total energies of MPcF<sub>4</sub>-p and MPcF<sub>4</sub>-np with ammonia molecules were carried out by the DFT method using the BP86 GGA functional [32,33], def2-SVP basis set of atomic orbitals [34], DFT-D3 dispersion interaction corrections [35,36], RI approximation [37–42], and the corresponding Def2/J auxiliary basis set [43]. The ORCA software package (version 5.0.2) was used for the calculations [44,45]. After optimizing the geometry of the compounds under consideration, their vibrational spectra were calculated to make sure that there were no negative frequencies and, as a result, that the calculated geometries corresponded to the ground states. The choice of the BP86 functional and the def2-SVP basis set was due to the fact that this combination allowed us to accurately describe the geometric structure of 3D metal complexes [46]. Visualization of the structure of the compounds under consideration was carried out using the ChemCraft program and the AIMStudio module of the AIMAll software package [47].

The location of four fluorine atoms in the peripheral and non-peripheral positions of cobalt phthalocyanine corresponded to the C<sub>s</sub> symmetry point group of both CoPcF<sub>4</sub>-p and CoPcF<sub>4</sub>-np molecules, since it was previously shown that the formation of these isomers was preferable to the molecules with D<sub>2h</sub>, C<sub>2v</sub>, or C<sub>4h</sub> symmetries [48]. However, symmetry constraints were not used during the calculations. The location of four fluorine atoms in the case of VOPcF<sub>4</sub>-np and VOPcF<sub>4</sub>-p was analogous (Figure 1). The spin multiplicity of all compounds, including those containing an ammonia molecule, was equal to two, so the calculations were performed in the framework of the spin-unrestricted Kohn–Sham theory (UKS).

After optimizing the geometry of the considered aggregates, the binding energy  $E_b$  of the NH<sub>3</sub> molecule with phthalocyanine was calculated from the difference in the total energies of both molecules separately, the geometry of which was also optimized, as well as their aggregate, as

$$E_b = E_{\text{NH}_3} + E_{\text{MPcF}_4-(\text{p})\text{np}} - E_{\text{MPcF}_4-(\text{p})\text{np}/\text{NH}_3} - \Delta E_{\text{BSSE}} \quad (1)$$

where  $\Delta E_{\text{BSSE}}$  is the correction to the binding energy, taking into account the basis set superposition error [49,50], which in turn was estimated as follows:

$$\Delta E_{\text{BSSE}} = \left( E_{\text{MPcF}_4-(\text{p})\text{np}}^* + E_{\text{NH}_3}^* \right) - \left( E_{\text{MPcF}_4-(\text{p})\text{np}^*} + E_{\text{NH}_3^*} \right) \quad (2)$$

Here, an asterisk in the superscript indicates that MPcF<sub>4</sub>-(p)np and NH<sub>3</sub> geometries, respectively, were taken from an optimized aggregate of phthalocyanine and ammonia molecules, while their geometry optimization was not carried out, but only the total energies calculation was performed. An asterisk in the subscript means that the indicated fragment of the whole aggregate was considered, while the points described by the corresponding basis sets of atomic orbitals were considered instead of the second fragment atoms.

Next, the electron wave functions of the optimized MPcF<sub>4</sub>-(p)np/NH<sub>3</sub> aggregates were calculated using the cc-pVTZ basis set of atomic orbitals [51]. Using these wave functions and the AIMAll software package [47], a topological analysis of the electron density distribution  $\rho(\mathbf{r})$  in the considered structures was performed in the framework of the QTAIM theory [52–54]. In particular, the values of  $\rho(\mathbf{r})$  and its Laplacian  $\nabla^2\rho(\mathbf{r})$  were obtained at bond critical points (BCPs), characterizing the interaction of ammonia molecules with phthalocyanine atoms.

## 3. Results

### 3.1. Characterization of MPcF<sub>4</sub> Films

XRD patterns of MPcF<sub>4</sub>-p and MPcF<sub>4</sub>-np thin films are shown in Figure 2. Diffraction patterns of all thin films except VOPcF<sub>4</sub>-np contain single strong diffraction peak in 6–7° 2 $\theta$  area, which may indicate a preferred orientation of crystallites within thin film. For the films of Cu, Co and Zn phthalocyanines (both –p and –np), the positions of diffraction

peaks match well with the first peak on their powder diffraction patterns calculated from respective crystal structure data [31,55,56]. An additional weak (0–12) diffraction peak is also visible on the diffraction pattern of a  $\text{CuPcF}_4$ -p film, indicating that its preferred orientation is weaker compared to others. The diffraction pattern of the  $\text{VOPcF}_4$ -p film also contains a second peak, but its corresponding interplanar distance is half of the position of the first peak, which means that both of these peaks belong to the same group of lattice planes, which is often observed for films with a strong preferred orientation. The positions of these peaks do not coincide with the calculated diffraction pattern, indicating that the  $\text{VOPcF}_4$ -p film consists of another crystalline phase with an unknown crystal structure [56]. On the other hand, the position of the diffraction peak observed on the  $\text{VOPcF}_4$ -np diffraction pattern coincides with the calculated diffraction patterns of both known  $\text{VOPcF}_4$ -np polymorphs (peak (–222) or (004)). However, both of these  $\text{VOPcF}_4$ -np polymorphs have a similar structure, with molecules packed in 2D layers, and these diffraction peaks correspond to the distance between these molecular layers.

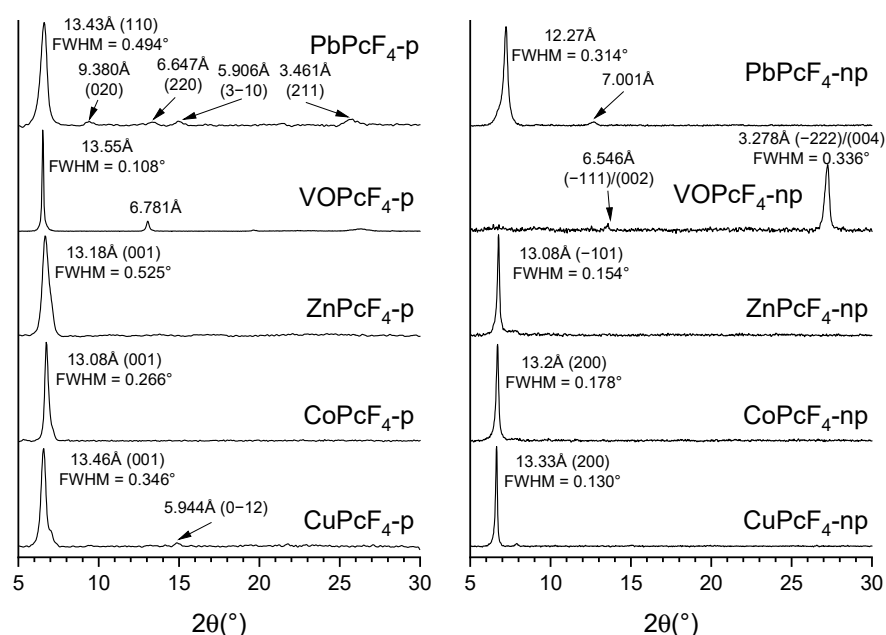


**Figure 2.** XRD patterns of  $\text{MPcF}_4$ -p and  $\text{MPcF}_4$ -np thin films in the  $2\theta$  range of 5–30°.

The X-ray pattern of the  $\text{PbPcF}_4$ -p film has several weak diffraction peaks in addition to the main peak, which coincide with the data of the single crystal [20]. This indicates a weak preferred orientation in the thin film. Finally, the diffractogram of the  $\text{PbPcF}_4$ -np film has one strong diffraction peak and one weak diffraction peak, neither of which correspond to the data of the single crystal. This means that the  $\text{PbPcF}_4$ -np film consists of an unknown crystalline phase but has a more preferred orientation compared to  $\text{PbPcF}_4$ -p.

Using the FWHM values of the observed diffraction peak, it is possible to estimate the size of the coherent scattering region for all investigated films using the Scherrer equation. Taking into account the instrumental broadening of the peak, which is 0.05° for the Bruker D8 advance powder diffractometer (measured using  $\text{LaB}_6$  SRM-660a powder as a reference), the coherent scattering regions are 30 nm for  $\text{CuPcF}_4$ -p, 41 nm for  $\text{CoPcF}_4$ -p, 19 nm for  $\text{ZnPcF}_4$ -p, 150 nm for  $\text{VOPcF}_4$ -p, and 20 nm for  $\text{PbPcF}_4$ -p. For  $\text{CuPcF}_4$ -np,  $\text{CoPcF}_4$ -np,  $\text{ZnPcF}_4$ -np,  $\text{VOPcF}_4$ -np, and  $\text{PbPcF}_4$ -np films, these values are 110 nm, 69 nm, 85 nm, 32 nm, and 34 nm, respectively.

Finally, knowing the plane of preferred orientation and the crystal structure of the film, it is possible to calculate the angle between the substrate surface and the phthalocyanine molecules inside the crystallites. The obtained inclination angles are 82.72° for  $\text{CuPcF}_4$ -p, 81.07° for  $\text{CoPcF}_4$ -p, 80.28° for  $\text{ZnPcF}_4$ -p, 90° for  $\text{PbPcF}_4$ -p (due to the tetragonal space

group),  $83.36^\circ$  and  $89.08^\circ$  for  $\text{CuPcF}_4\text{-np}$ ,  $78.15^\circ$  and  $80.99^\circ$  for  $\text{CoPcF}_4\text{-np}$ ,  $78.51^\circ$  for  $\text{ZnPcF}_4\text{-np}$  and  $0.39^\circ$  for  $\text{VOPcF}_4\text{-np}$ . Two values are given for  $\text{CuPcF}_4\text{-np}$  and  $\text{CoPcF}_4\text{-np}$ , since their crystal structures contain two symmetrically unequal molecules. A visual representation of the orientation of the molecules relative to the substrate surface is shown in Figure 3.

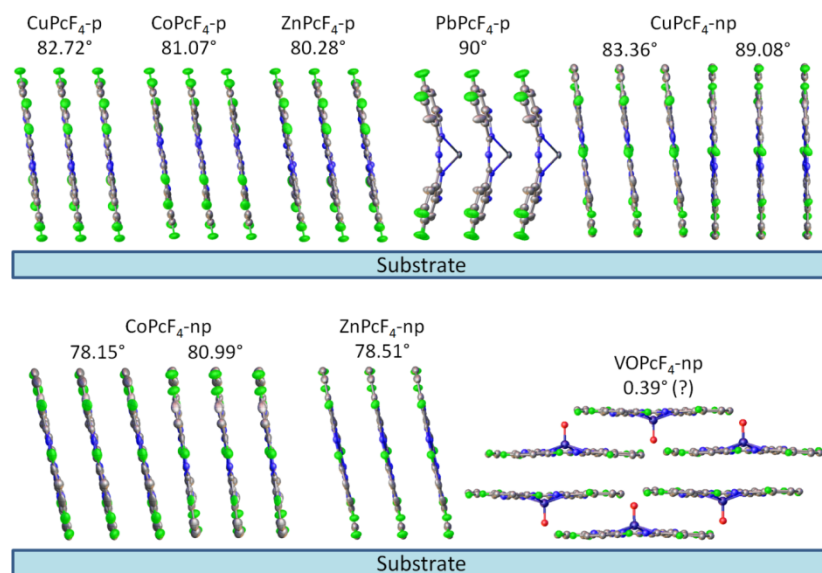


**Figure 3.** Orientation of  $\text{MPcF}_4\text{-p}$  and  $\text{MPcF}_4\text{-np}$  molecules relative to the substrate surface.

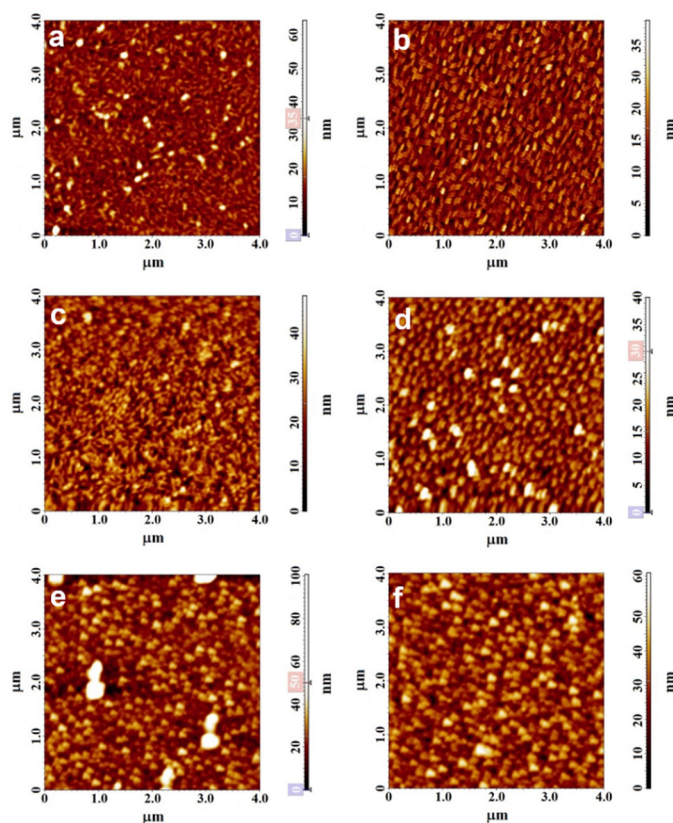
The morphology of the films was studied by atomic force microscopy. The AFM images of films of tetrafluorosubstituted phthalocyanines of cobalt, vanadyl and zinc are shown in Figure 4 as examples. The morphology of  $\text{CoPcF}_4\text{-np}$  and  $\text{CoPcF}_4\text{-p}$  films is very similar. The surface of  $\text{CoPcF}_4$  films is formed by elongated crystallites with a width of 50 to 100 nm and a length up to 200 nm. The root mean square (RMS) roughness is 4.04 nm and 4.18 nm for the  $\text{CoPcF}_4\text{-p}$  and  $\text{CoPcF}_4\text{-np}$  films, respectively. The  $\text{VOPcF}_4\text{-p}$  film is also formed by elongated crystallites that are oriented parallel to the substrate surface with their larger face, while in the  $\text{VOPcF}_4\text{-np}$  film, the crystallites are oriented almost perpendicular to the substrate surface. The RMS roughness of  $\text{VOPcF}_4\text{-p}$  and  $\text{VOPcF}_4\text{-np}$  films are 7.6 and 5.9 nm, respectively. The surface of both films of  $\text{ZnPcF}_4$  consists of slightly rounded crystallites with the size reaching 70 nm. The RMS roughness of  $\text{ZnPcF}_4\text{-np}$  and  $\text{ZnPcF}_4\text{-p}$  films are 9.54 and 4.44 nm, respectively.

### 3.2. Sensor Properties of $\text{MPcF}_4$ Films

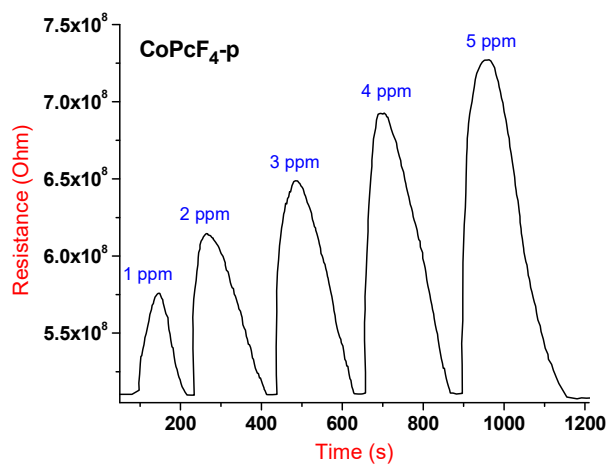
#### 3.2.1. Comparative Study of the Sensor Response of $\text{MPcF}_4\text{-p}$ and $\text{MPcF}_4\text{-np}$ Films to Ammonia

A typical chemiresistive sensor response, which is an increase in the resistance of the film when ammonia is injected into the cell and the resistance returns to its original value, after purging the cell with air, is shown in Figure 5 for the film of  $\text{CoPcF}_4\text{-p}$  as an example.

The films of all investigated  $\text{MPcF}_4\text{-p}$  and  $\text{MPcF}_4\text{-np}$  films demonstrate an increase in the resistance of the film when ammonia is injected into the cell, which is typical for metal phthalocyanines, exhibiting p-type semiconductor behavior [57]. When  $\text{NH}_3$  adsorption occurs on the surface of a phthalocyanine film, the electron density transfers from the  $\text{NH}_3$  molecule to the film. This reduces the concentration of the main charge carriers and increases the resistance. After purging the gas cell with air,  $\text{NH}_3$  removes from the film surface, which leads to a return of resistance to its initial value. The sensor response to ammonia in the investigated concentration range from 1 to 50 ppm is completely reversible at room temperature.

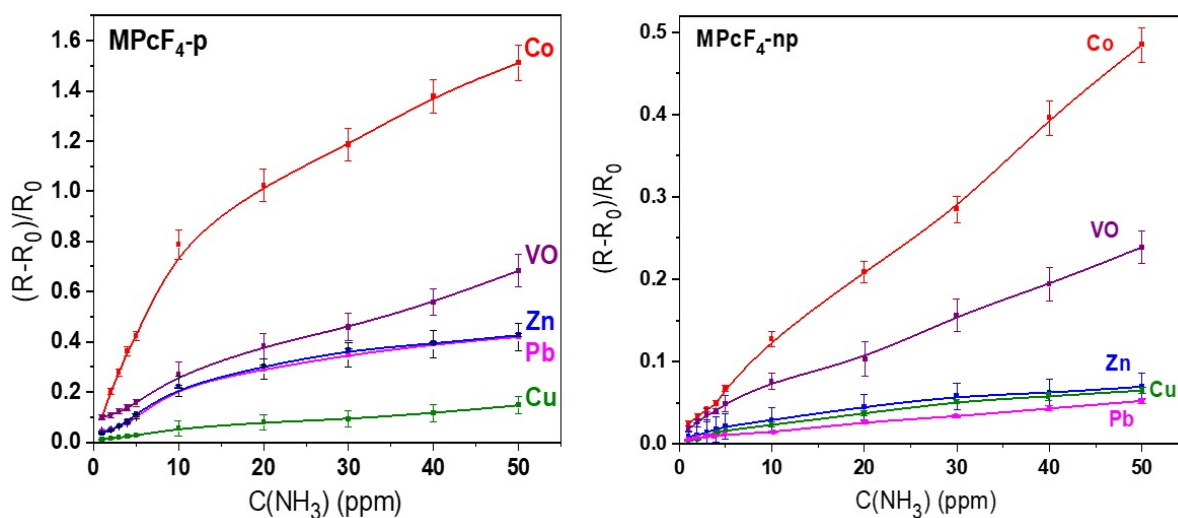


**Figure 4.** AFM images of CoPcF<sub>4</sub>-p (a), CoPcF<sub>4</sub>-np (b), VOPcF<sub>4</sub>-p (c), VOPcF<sub>4</sub>-np (d), ZnPcF<sub>4</sub>-p (e), and ZnPcF<sub>4</sub>-np (f) films.



**Figure 5.** Typical chemiresistive sensor response of a CoPcF<sub>4</sub>-p film to ammonia (1–5 ppm), measured at room temperature.

To compare the sensor properties of MPcF<sub>4</sub> with different central metals and positions of F-substituents, the sensor response of all films was measured at the same experimental conditions. The resulted dependencies of the value of the sensor response of all investigated films on ammonia concentration in the range from 1 to 50 ppm are shown in Figure 6.



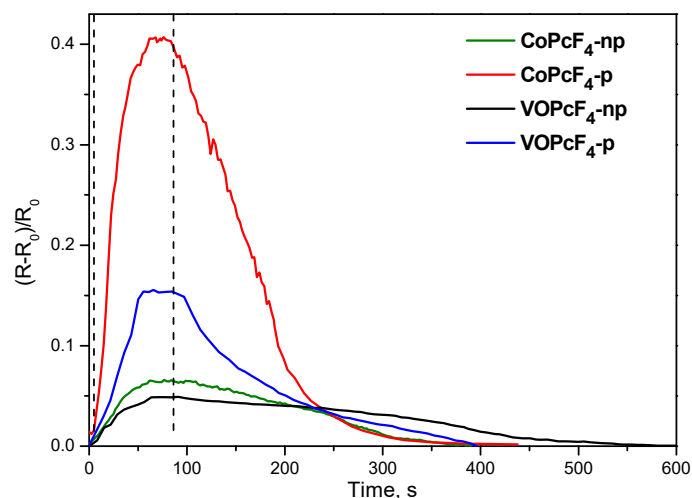
**Figure 6.** Dependence of the sensor response of MPcF<sub>4</sub>-p and MPcF<sub>4</sub>-np films on ammonia concentration (1–50 ppm), measured at room temperature.

Figure 6 shows that, in the case of MPcF<sub>4</sub>-p, the sensor response increases in the order CuPcF<sub>4</sub>-p < PbPcF<sub>4</sub>-p ~ ZnPcF<sub>4</sub>-p < VOPcF<sub>4</sub>-p < CoPcF<sub>4</sub>-p, while in the case of MPcF<sub>4</sub>-np the order is slightly different: PbPcF<sub>4</sub>-np < CuPcF<sub>4</sub>-np ~ ZnPcF<sub>4</sub>-np < VOPcF<sub>4</sub>-np < CoPcF<sub>4</sub>-np. For both types of substitution, cobalt phthalocyanine derivatives demonstrate the maximal value of the response to ammonia, followed by vanadyl phthalocyanines. The sensor response of cobalt phthalocyanine derivatives to 10 ppm NH<sub>3</sub> is more than 3–14 times higher than in the case of other MPcF<sub>4</sub>-p, and 1.5–10 times higher than in the case of other MPcF<sub>4</sub>-np, depending on the type of central metal ion. When comparing phthalocyanines with different positions of F-substituents in the macroring, MPcF<sub>4</sub>-p films exhibit a higher sensor response than MPcF<sub>4</sub>-np ones. For example, the sensor response of CoPcF<sub>4</sub>-p to 10 ppm NH<sub>3</sub> is about six times higher than that of CoPcF<sub>4</sub>-np.

All investigated phthalocyanine films demonstrate linear dependencies of the sensor response on ammonia concentration in the range from 1 to 10 ppm. The limits of ammonia detection (LOD), calculated as  $3\sigma/m$  ( $\sigma$  is the standard deviation of the sensor response to 1 ppm NH<sub>3</sub> and  $m$  is the slope of the calibration plot in the linear region of 1–10 ppm) are summarized in Table 1. The values of the response and recovery time determined upon exposure of the films with 5 ppm NH<sub>3</sub> (Figure 7) are also given in Table 1.

**Table 1.** Limits of ammonia detection (LOD), response and recovery times of MPcF<sub>4</sub>-p and MPcF<sub>4</sub>-np films.

Sensing Layer	LOD, ppm	Response Time, s (at 5 ppm)	Recovery Time, s (at 5 ppm)
CoPcF <sub>4</sub> -p	0.01	55	215
VOPcF <sub>4</sub> -p	0.04	48	270
ZnPcF <sub>4</sub> -p	0.01	45	210
PbPcF <sub>4</sub> -p	0.65	40	250
CuPcF <sub>4</sub> -p	0.75	40	240
CoPcF <sub>4</sub> -np	0.11	60	215
VOPcF <sub>4</sub> -np	0.87	62	350
ZnPcF <sub>4</sub> -np	0.08	35	155
PbPcF <sub>4</sub> -np	1.82	40	110
CuPcF <sub>4</sub> -np	1.49	55	90



**Figure 7.** Sensor response of  $MPcF_4-p$  and  $MPcF_4-np$  films ( $M = Co, VO$ ) to ammonia (5 ppm), measured at room temperature.

### 3.2.2. Quantum-Chemical Modeling of the Interaction of the $NH_3$ Molecule with Phthalocyanines

To explain the effect of the stronger sensor response of  $MPcF_4-p$  phthalocyanines compared to  $MPcF_4-np$  toward ammonia, quantum-chemical modeling of the interaction of the  $NH_3$  molecule with them was carried out. In this case, the complexes of cobalt and vanadyl, which are examples of phthalocyanines with a planar and non-planar structure, were considered.

Despite the fact that the bond of ammonia with the central metal in the phthalocyanine molecule is stronger, we considered the interaction of  $NH_3$  with the side atoms of the macrocycles (Figures 8 and 9). This choice of sites for the adsorption of  $NH_3$  molecules was due to two reasons. First, the strong binding of ammonia to metal atoms with the formation of a coordination bond complicates its desorption under normal conditions, and, as a consequence, can lead to an irreversible sensor response, which contradicts experimental data [29]. Second, the typical distance between phthalocyanine molecules in a stack is about 3.4 Å [55]. This is slightly larger than the van der Waals diameter of the nitrogen atom, and approximately equal to the diameter of the carbon atom, which is due to the  $\pi$ - $\pi$ -interaction between macrocycles. Therefore, there is not enough space for the ammonia molecule between two phthalocyanine macrocycles. That is precisely why the probability of the formation of a strong bond between a metal atom and the  $NH_3$  molecule is low. Moreover, Chia et al. [58] demonstrated that ammonia did not interact with the metal center of the unsubstituted copper phthalocyanine, using the methods of in situ X-ray absorption spectroscopy (XAS) and EXAFS. The EXAFS study showed that the interaction occurred at the benzene ring or bridging nitrogen atom of the macrocycle. We have previously proposed and considered the mechanism of the sensor response of hybrids of carbon nanotubes with phthalocyanines, which is associated with a decrease in their electrical conductivity during the formation of hydrogen bonds between the ammonia molecule and side atoms of phthalocyanines [59].

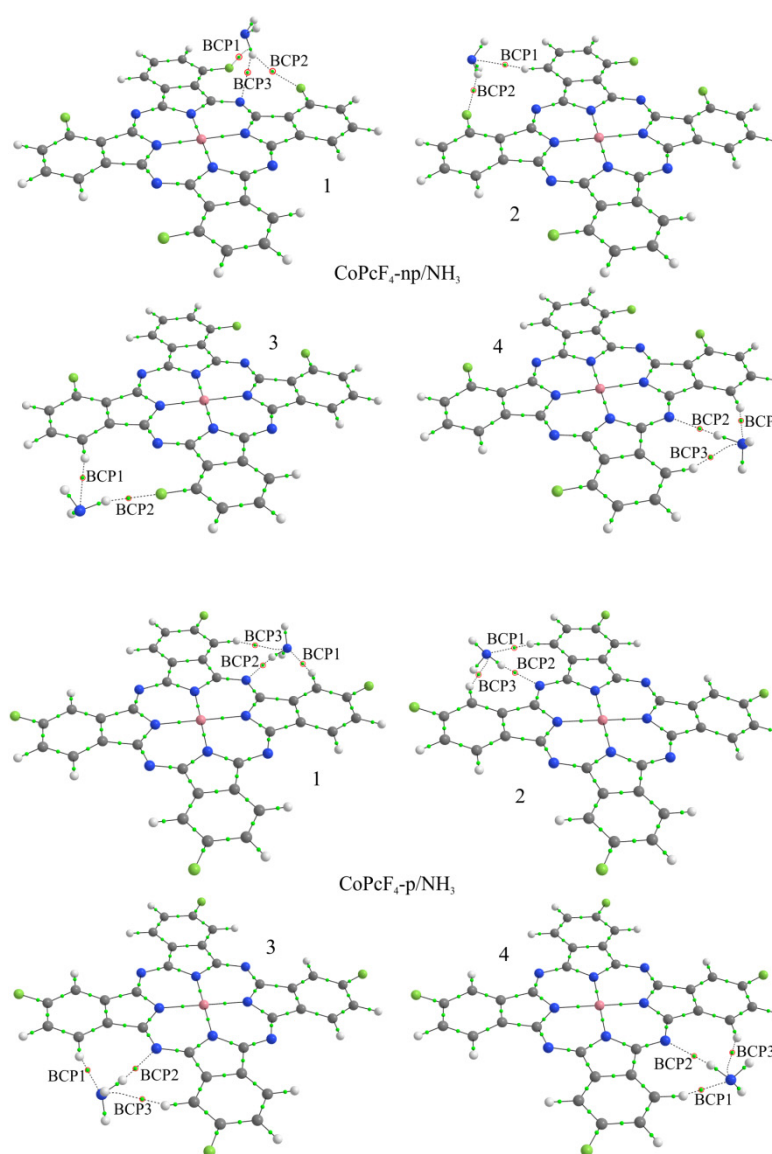


**Figure 8.** Structure of CoPcF<sub>4</sub>-np/NH<sub>3</sub> and CoPcF<sub>4</sub>-p/NH<sub>3</sub> aggregates and bond critical points (BCP) in them. Red circles indicate BCPs characterizing the interaction of the ammonia molecule with phthalocyanine atoms.

In the process of geometry optimization, it was found that in all cases, except for VOPcF<sub>4</sub>-np/NH<sub>3</sub>-1 and CoPcF<sub>4</sub>-np/NH<sub>3</sub>-1, the NH<sub>3</sub> molecule occupies an equilibrium position in such a way that its nitrogen atom is approximately in the same plane as the phthalocyanine molecule. In this case, the distance of ammonia from the macrocycle can be characterized using the distance  $d$  between the nitrogen atom of the NH<sub>3</sub> molecule and the nearest bridging nitrogen atom of phthalocyanine (Tables 2 and 3). In the case of VOPcF<sub>4</sub>-np/NH<sub>3</sub>-1 and CoPcF<sub>4</sub>-np/NH<sub>3</sub>-1, the ammonia molecule occupies an equilibrium position above the macrocycle plane, which contradicts the above idea that this molecule cannot fit into the space between two adjacent phthalocyanines in the stack. Therefore, these two aggregates were excluded from further consideration.

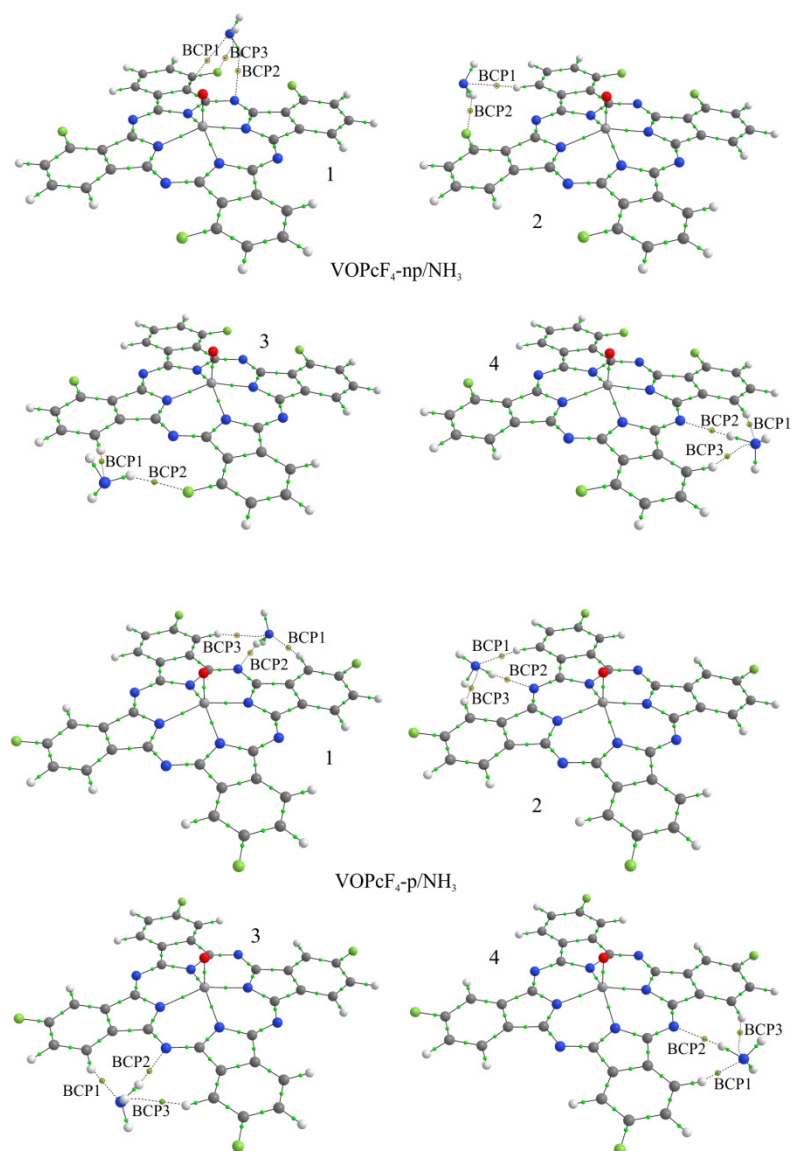


**Figure 9.** Structure of VOPcF<sub>4</sub>-np/NH<sub>3</sub> and VOPcF<sub>4</sub>-p/NH<sub>3</sub> aggregates and bond critical points in them. Red circles indicate BCPs characterizing the interaction of the ammonia molecule with phthalocyanine atoms.

**Table 2.** The interaction parameters of the NH<sub>3</sub> molecule with cobalt phthalocyanines.

Compound	$E_b$ , eV	$d$ , Å	BCP	Atoms *	$\rho(r)$ , e/Å <sup>3</sup>	$\nabla^2\rho(r)$ , e/Å <sup>5</sup>
CoPcF <sub>4</sub> -np/NH <sub>3</sub> -2	0.036	4.251	1	H-N	0.083	0.880
			2	F-H	0.066	1.058
CoPcF <sub>4</sub> -np/NH <sub>3</sub> -3	0.035	4.270	1	H-N	0.083	0.885
			2	F-H	0.066	1.060
CoPcF <sub>4</sub> -np/NH <sub>3</sub> -4	0.130	3.236	1	H-N	0.137	1.526
			2	N-H	0.123	1.238
			3	H-N	0.099	1.070
CoPcF <sub>4</sub> -p/NH <sub>3</sub> -1	0.160	3.192	1	H-N	0.146	1.567
			2	N-H	0.135	1.334
			3	H-N	0.094	1.009

**Table 2.** *Cont.*

Compound	$E_b$ , eV	$d$ , Å	BCP	Atoms *	$\rho(r)$ , $e/\text{Å}^3$	$\nabla^2\rho(r)$ , $e/\text{Å}^5$
CoPcF <sub>4</sub> -p/NH <sub>3</sub> -2	0.161	3.209	1	H-N	0.137	1.502
			2	N-H	0.131	1.300
			3	H-N	0.095	1.023
CoPcF <sub>4</sub> -p/NH <sub>3</sub> -3	0.162	3.207	1	H-N	0.137	1.504
			2	N-H	0.131	1.304
			3	H-N	0.095	1.023
CoPcF <sub>4</sub> -p/NH <sub>3</sub> -4	0.158	3.203	1	H-N	0.138	1.516
			2	N-H	0.133	1.312
			3	H-N	0.093	1.005

\* The first atom belongs to the phthalocyanine molecule and the second one belongs to the ammonia molecule.

**Table 3.** The interaction parameters of the NH<sub>3</sub> molecule with vanadyl phthalocyanines.

Compound	$E_b$ , eV	$d$ , Å	BCP	Atoms *	$\rho(r)$ , $e/\text{Å}^3$	$\nabla^2\rho(r)$ , $e/\text{Å}^5$
VOPcF <sub>4</sub> -np/NH <sub>3</sub> -2	0.035	4.213	1	H-N	0.085	0.904
			2	F-H	0.065	1.050
VOPcF <sub>4</sub> -np/NH <sub>3</sub> -3	0.034	4.220	1	H-N	0.085	0.904
			2	F-H	0.065	1.053
VOPcF <sub>4</sub> -np/NH <sub>3</sub> -4	0.144	3.227	1	H-N	0.137	1.519
			2	N-H	0.125	1.256
			3	H-N	0.096	1.038
VOPcF <sub>4</sub> -p/NH <sub>3</sub> -1	0.174	3.179	1	H-N	0.148	1.570
			2	N-H	0.139	1.360
			3	H-N	0.091	0.979
VOPcF <sub>4</sub> -p/NH <sub>3</sub> -2	0.173	3.196	1	H-N	0.138	1.502
			2	N-H	0.135	1.327
			3	H-N	0.093	0.997
VOPcF <sub>4</sub> -p/NH <sub>3</sub> -3	0.173	3.195	1	H-N	0.138	1.504
			2	N-H	0.135	1.328
			3	H-N	0.092	0.996
VOPcF <sub>4</sub> -p/NH <sub>3</sub> -4	0.170	3.190	1	H-N	0.140	1.518
			2	N-H	0.137	1.338
			3	H-N	0.091	0.980

\* The first atom belongs to the phthalocyanine molecule and the second one belongs to the ammonia molecule.

The binding energy in CoPcF<sub>4</sub>-p/NH<sub>3</sub>- $x$  ( $x = 1-4$ , Figures 8 and 9) aggregates varies from 0.158 eV to 0.161 eV, which exceeds the values of 0.035–0.130 eV obtained for CoPcF<sub>4</sub>-np/NH<sub>3</sub>- $x$  ( $x = 2-4$ ) (Tables 2 and 3). Stronger binding of the NH<sub>3</sub> molecule has a stronger effect on the electronic structure of phthalocyanine and, as a result, on the conductivity of the macrocycle stack. At the same time, in the case of the peripheral position of F-substituents, the ammonia molecule is located deeper in the cavity between adjacent benzene rings and closer to the bridging nitrogen atom; that is,  $d$  varies in the range of 3.192–3.209 Å. In the case of a non-peripheral position of the F-substituents, this distance is larger and equal to 3.236–4.270 Å.

The CoPcF<sub>4</sub>-np/NH<sub>3</sub>-4 aggregate, in which there are no fluorine atoms in the cavity where the ammonia molecule is embedded, should be separately noted. This arrangement allows the ammonia to approach the phthalocyanine nitrogen bridge atom in such a way that the corresponding distance  $d$  is 3.236 Å, and the binding energy is 0.130 eV. These values are close to those obtained for all four CoPcF<sub>4</sub>-p/NH<sub>3</sub>- $x$  aggregates. This means that fluorine atoms in non-peripheral positions, due to their size and the larger carbon-fluorine distance compared to the carbon–hydrogen distance, prevent the NH<sub>3</sub> molecule from

approaching the macrocycle closely, which causes a weaker binding of ammonia and its lesser effect on the electronic phthalocyanine structure.

The topological analysis of the electron density distribution in aggregates with CoPcF<sub>4</sub> made it possible to find the bond critical points between the atoms of ammonia and phthalocyanine (Figure 8). In particular, it was shown that in all cases of CoPcF<sub>4</sub>-p/NH<sub>3</sub>-*x* there are three such points, two of which (BCP1 and BCP3) are located between the hydrogen atoms of phthalocyanine and the nitrogen atom of the NH<sub>3</sub> molecule, and one (BCP2), on the contrary, between one of the ammonia hydrogen atoms and the bridging nitrogen atom of phthalocyanine. A similar situation is observed in the case of CoPcF<sub>4</sub>-np/NH<sub>3</sub>-4. The values of  $\rho(\mathbf{r})$  and  $\nabla^2\rho(\mathbf{r})$  at these points are in the ranges of 0.093–0.146  $e/\text{\AA}^3$  and 1.005–1.567  $e/\text{\AA}^5$  (Table 1), respectively. This indicates the formation of hydrogen bonds between the ammonia and phthalocyanine molecules since it was previously shown that the criterion for this is the values of the electron density and its Laplacian in the ranges of 0.013–0.236  $e/\text{\AA}^3$  and 0.578–3.350  $e/\text{\AA}^5$  [60].

Since the fluorine atoms in the considered phthalocyanine molecules are located asymmetrically relative to the rotation axis passing perpendicular to the macrocycle plane through the metal atom, there are four nonequivalent sites for attaching the NH<sub>3</sub> molecule in each phthalocyanine. These sites are located between adjacent benzene rings opposite the bridging nitrogen atom. Consequently, in the case of each phthalocyanine, all four positions of the attachment of ammonia molecule were considered, and the corresponding aggregates were further designated as MPcF<sub>4</sub>-p/NH<sub>3</sub>-*x* or MPcF<sub>4</sub>-np/NH<sub>3</sub>-*x*, where *x* = 1, 2, 3, or 4 (Figures 8 and 9).

In the case of the CoPcF<sub>4</sub>-np/NH<sub>3</sub>-2 and CoPcF<sub>4</sub>-np/NH<sub>3</sub>-3 aggregates, the interaction of the NH<sub>3</sub> molecule with phthalocyanines can be characterized by the presence of two BCPs: the first one (BCP1) is between the phthalocyanine hydrogen atom and the ammonia nitrogen atom, and the second one (BCP2) is between the phthalocyanine fluorine atom and one of the ammonia hydrogen atoms (Figure 8). The values of  $\rho(\mathbf{r})$  and  $\nabla^2\rho(\mathbf{r})$  at these points are significantly lower than in the case of CoPcF<sub>4</sub>-p/NH<sub>3</sub>-*x*, which is consistent with the lower  $E_b$  values, but they also indicate the formation of hydrogen bonds.

The results of quantum-chemical calculations of the VOPcF<sub>4</sub>-np/NH<sub>3</sub> and VOPcF<sub>4</sub>-p/NH<sub>3</sub> aggregates are almost completely equivalent to those obtained for the cobalt complexes, namely the binding energy of NH<sub>3</sub> with VOPcF<sub>4</sub>-p is higher than in the case of VOPcF<sub>4</sub>-np derivative. The topological analysis of the electron density distribution in the VOPcF<sub>4</sub>-np/NH<sub>3</sub> and VOPcF<sub>4</sub>-p/NH<sub>3</sub> aggregates showed that the values of  $\rho(\mathbf{r})$  and  $\nabla^2\rho(\mathbf{r})$  at the bond critical points between the ammonia and phthalocyanine atoms are close to those obtained in the case of cobalt complexes. Consequently, the formation of hydrogen bonds is also observed during the interaction of the NH<sub>3</sub> molecule with the side atoms of vanadyl phthalocyanines. However, it is necessary to mention that the binding energy values in the VOPcF<sub>4</sub>-p/NH<sub>3</sub>-*x* and VOPcF<sub>4</sub>-np/NH<sub>3</sub>-4 aggregates (Table 3) are slightly higher than in the case of the corresponding cobalt phthalocyanine derivatives.

If we compare the calculation data with the data of the experimental study of the sensor response, it can be noted that the sensor response of VOPcF<sub>4</sub> derivatives, on the contrary, is lower than CoPcF<sub>4</sub>, whereas their relaxation time is higher in the case of CoPcF<sub>4</sub>. It should be noted here that the bond strength is not the only factor affecting the sensor response. The proposed model is applicable only to explain the effect of the position of substituents on the value of the sensor response; however, it does not allow for taking into account the influence of the central metal. Perhaps this was due to the fact that an isolated phthalocyanine molecule was considered. In crystals and films, phthalocyanine molecules are packed in stacks and the conductivity of the films and charge transfer are determined by intermolecular interactions. Taking into account the different packing of cobalt and vanadyl phthalocyanines, ways of overlapping  $\pi$ -orbitals of neighboring macrocycles, and the nature and location of the central metals, it can be assumed that the charge transfer processes in these structures as a result of ammonia adsorption will differ. This issue requires further in-depth consideration, and, apparently, quantum chemical calculations of

individual molecules will not be enough. Therefore, in the future, in order to consider the influence of various central metals on the sensor response, it will be necessary to model stacks of phthalocyanine molecules in the form of large clusters or periodic structures.

These statements are also confirmed by additional quantum-chemical calculations of the binding energy of the ammonia molecule with other phthalocyanines  $MPcF_4-p$  and  $MPcF_4-np$ , where  $M = Cu, Zn, \text{ and } Pb$ , performed using the same approach. The results are similar to those observed in the case of cobalt and vanadyl phthalocyanines. Firstly, the peripheral positions of fluorine atoms are a more favorable factor for the stronger binding of the  $NH_3$  molecule than the non-peripheral positions (Table 4). Secondly, the binding energies of the ammonia molecule with  $MPcF_4-p$  and  $MPcF_4-np$  where  $M = Cu, Zn, \text{ and } Pb$  are close to those obtained in the case of cobalt and vanadyl phthalocyanines. Thirdly, when passing from one metal phthalocyanine to another, the tendency of changing  $E_b$  values does not agree with the experimentally established order, changing the value of the sensor response.

**Table 4.** The binding energies (in eV) of the  $NH_3$  molecule with  $MPcF_4$  ( $M = Cu, Zn, Pb$ ) phthalocyanines.

Compound	$NH_3$ Position	$M = Cu$	$M = Zn$	$M = Pb$
$MPcF_4-np/NH_3$	2	0.037	0.037	-
	3	0.036	0.036	-
	4	0.145	0.151	0.144
$MPcF_4-p/NH_3$	1	0.172	0.179	0.173
	2	0.172	0.179	0.172
	3	0.173	0.179	0.172
	4	0.169	0.176	0.169

It is necessary to mention that, in the case of lead phthalocyanines, the planar structure of the macrocycle is strongly distorted. For this reason, the size of the cavities in which the location of ammonia is considered decreases. As a result, the  $NH_3$  molecule cannot be localized in positions two and three, where fluorine atoms are present, and in the process of geometry optimization, a structure with  $NH_3$  above the macrocycle is formed as shown in Figure 10. For this reason, the binding energies of  $NH_3$  in  $PbPcF_4-np/NH_3-2$  and  $PbPcF_4-np/NH_3-3$  aggregates were not calculated (Table 4).

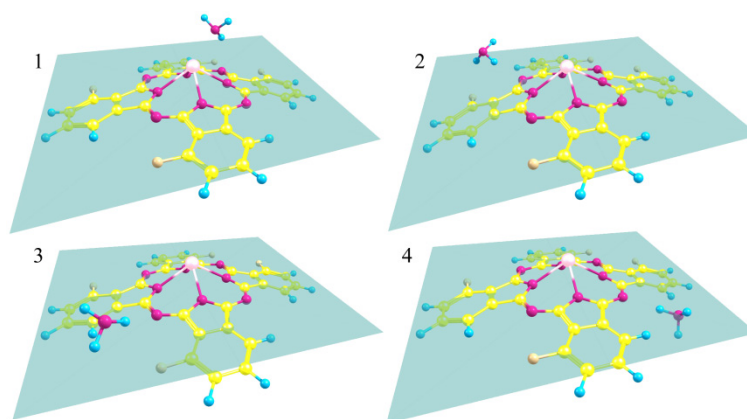


**Figure 10.** Structure of  $PbPcF_4-np/NH_3$  aggregates. The indicated plane passes through bridge nitrogen atoms to show the position of the  $NH_3$  molecule relative phthalocyanine surface, numbers 1–4 indicate type of aggregate.

Thus, there are significantly fewer places for ammonia adsorption in  $PbPcF_4-np$  than in all other  $MPcF_4-np$ , and attachment can occur only at position four (Figure 10), at which there are no fluorine atoms in the considered cavity. This result is consistent with the fact that  $PbPcF_4-np$  films have the lowest sensor response in the experiment.

### 3.2.3. Detailed Study of the Sensor Characteristics of MPcF<sub>4</sub>-p (M = Co, VO) Films to Ammonia

For the films of CoPcF<sub>4</sub>-p and VOPcF<sub>4</sub>-p, which demonstrate the highest sensor response among those investigated, the more detailed investigation of the sensor properties was carried out. Figure 11 shows the sensor response of CoPcF<sub>4</sub>-p and VOPcF<sub>4</sub>-p films to ammonia (3 ppm) and the change in their resistance at a different relative humidity (RH). An increase in RH causes a growth of the films' resistance, since, like ammonia, water is an electron donating molecule. At the same time, an increase in RH up to 40% does not affect the base resistance and the response, while an increase in humidity up to 80% results in a noticeable (1.6 time for a CoPcF<sub>4</sub>-p film and 4.7 time for a VOPcF<sub>4</sub>-p film) increase in the sensor response.

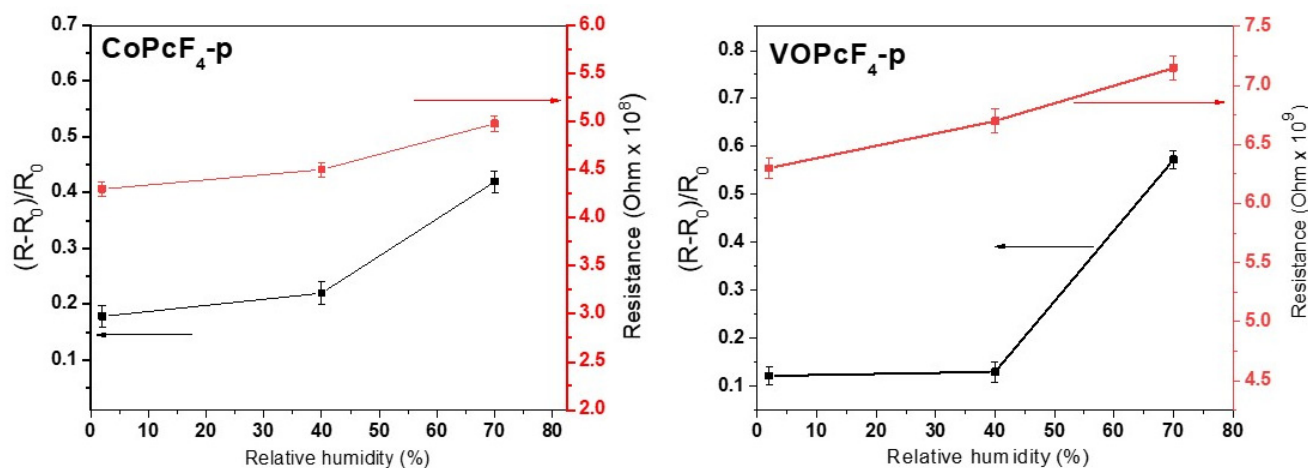


**Figure 11.** The sensor response of CoPcF<sub>4</sub>-p and VOPcF<sub>4</sub>-p films to ammonia (3 ppm) and the change in their resistance at different humidity.

The operating temperature is a unique characteristic of each sensor. The sensor response of cobalt and vanadyl phthalocyanine layers to ammonia was tested at 25, 40, and 80 °C. An increase in temperature leads to an increase in response (Figure 12). This behavior appears to be associated with an increase in the concentration of charge carriers in p-type semiconductors with an increase in temperature [61]. The increase in the concentration of charge carriers is also confirmed by a slight decrease in base films resistance of the films with temperature. An increase in the operating temperature activates the desorption process, which leads to a decrease in response time. For example, in the case of CoPcF<sub>4</sub>-p, when the operating temperature increases from 25 to 80 °C, the recovery time decreases from 215 to 145 s.

The stability and repeatability of the sensor based on cobalt and vanadyl phthalocyanines were also tested. The sensor response of a fresh CoPcF<sub>4</sub>-p film to 3 ppm of ammonia and the same film after 7, 14, 28, and 120 days is shown in Figure 13a as an example. The change in both the sensor response and the base resistance does not exceed the measurement error, which indicates good repeatability and long-term stability of the investigated sensing layer.

To investigate the selectivity with respect to NH<sub>3</sub>, the response of MPcF<sub>4</sub> layers toward other gaseous analytes was studied (Figure 13b). Pure dry NH<sub>3</sub>, CO<sub>2</sub>, and H<sub>2</sub>S were used as analytes. Ethanol, acetone, benzene, and formaldehyde vapors were generated by evaporation of their liquids using an evaporator located inside the test chamber.

It was found that, among reducing gases and volatile organic vapors, the layers exhibited the maximal response to ammonia, but at a concentration of more than 10 ppm, hydrogen sulfide can act as an interfering gas.

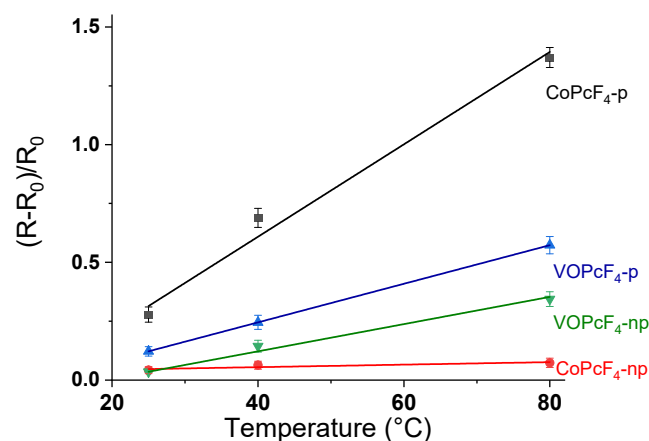


**Figure 12.** Sensor response of an MPcF<sub>4</sub>-p and MPcF<sub>4</sub>-np (M = Co, VO) layer to ammonia (3 ppm) measured at 25, 40 and 80 °C.

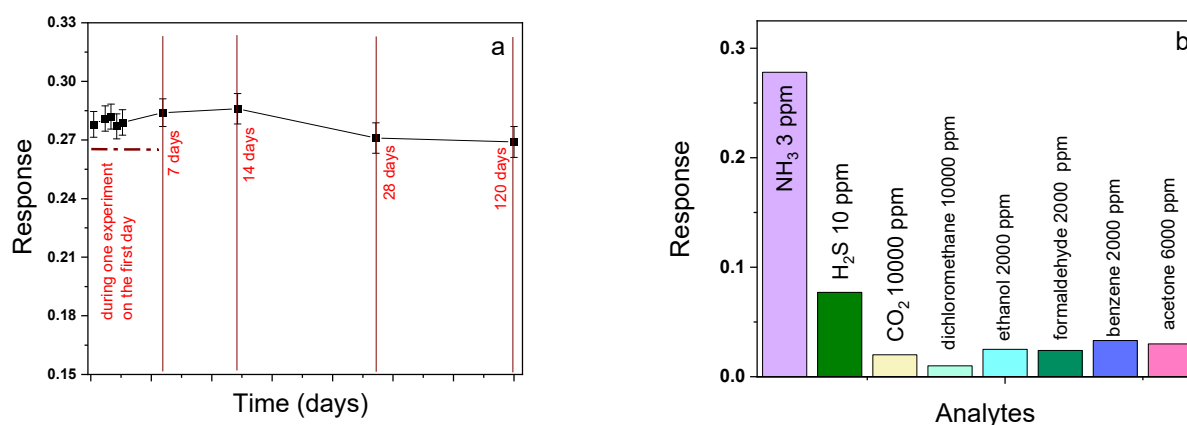


**Figure 13.** (a) Sensor response of a CoPcF<sub>4</sub>-p film to ammonia (3 ppm) after 7, 14, 28, and 120 days. (b) Diagram of sensitivity of a CoPcF<sub>4</sub>-p film to various gaseous analytes and volatile organic vapors.

Table 5 shows the sensor properties of CoPcF<sub>4</sub> films in comparison with the characteristics of some chemiresistive sensors to ammonia described in the literature [62–65]. The presented sensor characteristics of a CoPcF<sub>4</sub>-p film are comparable to or even exceed the characteristics of sensors based on semiconductor oxides and nanomaterials listed in Table 5. Thus, active layers based on CoPcF<sub>4</sub>-p and VOPcF<sub>4</sub>-p are promising materials for creating sensors for the detection of low concentrations of ammonia in the air.

**Table 5.** Sensor characteristics of various chemiresistive sensors to ammonia.

Material	Concentration Range, ppm	LOD, ppm	Response, %	Response/Recovery Time, s	Ref.
polyimide-SnO <sub>2</sub> /rGO	50–800	15	5.16 (100 ppm)	94/57	[62]
MXene/Graphene composite	0.5–100	0.056	25 (100 ppm)	26/148	[63]
ZnO and WO <sub>3</sub> ·H <sub>2</sub> O composite	2–100	0.76	~15 (10 ppm)	2.4/1.2	[64]
SWCNT-TiOPc	5–50	n/a	1.76 (50 ppm)	120 (fixed)/~40	[65]
CoPcF <sub>4</sub> -p	1–50	0.01	42 (5 ppm)	55/215	Our work
VOPcF <sub>4</sub> -p	1–50	0.04	15 (5 ppm)	48/270	Our work

#### 4. Conclusions

A comparative analysis of the chemiresistive sensor response of thin films of a series of tetrasubstituted phthalocyanine of various metals with F-substituent in peripheral (MPcF<sub>4</sub>-p, M = Cu, Co, Zn, Pb, VO) and non-peripheral (MPcF<sub>4</sub>-np) positions in macroring to low concentrations of ammonia (1–50 ppm) was carried out. It was found that, in the case of MPcF<sub>4</sub>-p, the sensor response increases in the order CuPcF<sub>4</sub>-p < PbPcF<sub>4</sub>-p ~ ZnPcF<sub>4</sub>-p < VOPcF<sub>4</sub>-p < CoPcF<sub>4</sub>-p, while in the case of MPcF<sub>4</sub>-np the order is slightly different: PbPcF<sub>4</sub>-np < CuPcF<sub>4</sub>-np ~ ZnPcF<sub>4</sub>-np < VOPcF<sub>4</sub>-np < CoPcF<sub>4</sub>-np. When comparing phthalocyanines with different positions of F-substituents in the macroring, MPcF<sub>4</sub>-p films exhibit a higher sensor response than MPcF<sub>4</sub>-np ones. The sensor response to ammonia was completely reversible at room temperature. For the films of CoPcF<sub>4</sub>-p and VOPcF<sub>4</sub>-p, which demonstrate the highest sensor response among those investigated, the more detailed investigation of the sensor properties was carried out. It was shown that a CoPcF<sub>4</sub>-p film demonstrated the calculated LOD of 0.01 ppm with the recovery time of 215 s, while a VOPcF<sub>4</sub>-p film had a LOD of 0.04 ppm and the recovery time of 270 s. Both sensors had good repeatability and long-term stability. The selectivity test showed that CO<sub>2</sub>, ethanol, acetone, benzene, and formaldehyde did not interfere with the determination of ammonia, while H<sub>2</sub>S at the concentration more than 10 ppm could act as an interfering gas.

It was shown as a result of quantum-chemical modeling that the observed regularities are best described by the interaction of an ammonia molecule with cobalt and vanadyl phthalocyanines through the formation of hydrogen bonds between NH<sub>3</sub> and side atoms of the phthalocyanine. In the case of phthalocyanine with a peripheral position of F-substituents, the NH<sub>3</sub> molecule approaches the macrocycle more closely and binds more strongly than in the case of phthalocyanines with non-peripheral positions of F-substituents. The stronger binding leads to a stronger effect of the ammonia molecule on the electronic structure of phthalocyanine and, as a consequence, on the electrical conductivity of the film. This, in turn, causes a stronger sensor response of MPcF<sub>4</sub>-p films to ammonia than in the case of MPcF<sub>4</sub>-np ones. However, the proposed model is applicable only for explaining the effect of the position of substituents on the value of the sensor response; it does not allow for taking into account the influence of the central metal. Perhaps this was due to the fact that an isolated phthalocyanine molecule was considered. Therefore, in the future, in order to consider the effect of central metals on the sensor response, it will be necessary to model stacks of phthalocyanine molecules in the form of large clusters or periodic structures.

**Author Contributions:** Conceptualization, P.K. and T.B.; methodology, P.K. and T.B.; software, P.K.; validation, P.K. and D.K.; formal analysis, P.K., D.K. and A.S.; investigation, P.K., A.S., D.K., P.P. and D.B.; resources, D.K.; writing—original draft preparation, D.K., P.P. and T.B.; writing—review and editing, D.K., P.P. and T.B.; visualization, D.B. and P.K.; supervision, T.B.; project administration, D.K.; funding acquisition, D.K. All authors have read and agreed to the published version of the manuscript.

**Funding:** The study of the films of lead and vanadyl phthalocyanines derivatives was funded by the Russian Science Foundation, grant number 22-73-00145. The study of the cobalt and copper phthalocyanine films was funded by the Ministry of Science and Higher Education of the Russian Federation, N 121031700314-5 and N 121031700313-8.

**Institutional Review Board Statement:** Not applicable.

**Informed Consent Statement:** Not applicable.

**Data Availability Statement:** Not applicable.

**Conflicts of Interest:** The authors declare no conflict of interest.

## References

1. Wang, H.; Zhang, Y.; Han, Q.; Xu, Y.; Hu, G.; Xing, H. The inflammatory injury of heart caused by ammonia is realized by oxidative stress and abnormal energy metabolism activating inflammatory pathway. *Sci. Total Environ.* **2020**, *742*, 140532. [[CrossRef](#)] [[PubMed](#)]
2. He, K.; Luo, X.; Wen, M.; Wang, C.; Qin, C.; Shao, J.; Gan, L.; Dong, R.; Jiang, H. Effect of acute ammonia toxicity on inflammation, oxidative stress and apoptosis in head kidney macrophage of *Pelteobagrus fulvidraco* and the alleviation of curcumin. *Comp. Biochem. Physiol. Part C Toxicol. Pharmacol.* **2021**, *248*, 109098. [[CrossRef](#)] [[PubMed](#)]
3. Vuppaladadiyam, A.K.; Antunes, E.; Vuppaladadiyam, S.S.V.; Baig, Z.T.; Subiantoro, A.; Lei, G.; Leu, S.Y.; Sarmah, A.K.; Duan, H. Progress in the development and use of refrigerants and unintended environmental consequences. *Sci. Total Environ.* **2022**, *823*, 153670. [[CrossRef](#)] [[PubMed](#)]
4. Insausti, M.; Timmis, R.; Kinnersley, R.; Rufino, M.C. Advances in sensing ammonia from agricultural sources. *Sci. Total Environ.* **2020**, *706*, 135124. [[CrossRef](#)]
5. Kwak, D.; Lei, Y.; Maric, R. Ammonia gas sensors: A comprehensive review. *Talanta* **2019**, *204*, 713–730. [[CrossRef](#)]
6. Wyer, K.E.; Kelleghan, D.B.; Blanes-Vidal, V.; Schaubberger, G.; Curran, T.P. Ammonia emissions from agriculture and their contribution to fine particulate matter: A review of implications for human health. *J. Environ. Manage.* **2022**, *323*, 116285. [[CrossRef](#)]
7. Kumar, V.; Mirzaei, A.; Bonyani, M.; Kim, K.H.; Kim, H.W.; Kim, S.S. Advances in electrospun nanofiber fabrication for polyaniline (PANI)-based chemoresistive sensors for gaseous ammonia. *TrAC Trends Anal. Chem.* **2020**, *129*, 115938. [[CrossRef](#)]
8. Brannelly, N.T.; Hamilton-Shield, J.P.; Killard, A.J. The Measurement of Ammonia in Human Breath and its Potential in Clinical Diagnostics. *Crit. Rev. Anal. Chem.* **2016**, *46*, 490–501. [[CrossRef](#)]
9. Song, G.; Jiang, D.; Wu, J.; Sun, X.; Deng, M.; Wang, L.; Hao, C.; Shi, J.; Liu, H.; Tian, Y.; et al. An ultrasensitive fluorescent breath ammonia sensor for noninvasive diagnosis of chronic kidney disease and helicobacter pylori infection. *Chem. Eng. J.* **2022**, *440*, 135979. [[CrossRef](#)]
10. Shetty, S.S.; Jayarama, A.; Bhat, S.; Karunasagar, I.; Pinto, R. A review on metal-oxide based trace ammonia sensor for detection of renal disease by exhaled breath analysis. *Mater. Today Proc.* **2022**, *55*, 113–117. [[CrossRef](#)]
11. Kim, K.-H.; Jahan, S.A.; Kabir, E. A review of breath analysis for diagnosis of human health. *TrAC Trends Anal. Chem.* **2012**, *33*, 1–8. [[CrossRef](#)]
12. Wang, G.; Gao, J.; Sun, B.; He, D.; Zhao, C.; Suo, H. Enhanced ammonia sensitivity electrochemical sensors based on PtCu alloy nanoparticles in-situ synthesized on carbon cloth electrode. *J. Electroanal. Chem.* **2022**, *922*, 116721. [[CrossRef](#)]
13. Tsai, J.-H.; Niu, J.-S.; Shao, W.-C.; Liu, W.-C. Characteristics of chemiresistive-type ammonia sensor based on Ga<sub>2</sub>O<sub>3</sub> thin film functionalized with platinum nanoparticles. *Sens. Actuators B Chem.* **2022**, *371*, 132589. [[CrossRef](#)]
14. Krishna, K.G.; Parne, S.; Pothukanuri, N.; Kathirvelu, V.; Gandhi, S.; Joshi, D. Nanostructured metal oxide semiconductor-based gas sensors: A comprehensive review. *Sens. Actuators A Phys.* **2022**, *341*, 113578. [[CrossRef](#)]
15. Ma, J.; Fan, H.; Li, Z.; Jia, Y.; Yadav, A.K.; Dong, G.; Wang, W.; Dong, W.; Wang, S. Multi-walled carbon nanotubes/polyaniline on the ethylenediamine modified polyethylene terephthalate fibers for a flexible room temperature ammonia gas sensor with high responses. *Sens. Actuators B Chem.* **2021**, *334*, 129677. [[CrossRef](#)]
16. Ganesan, S.; Kalimuthu, R.; Kanagaraj, T.; Kulandaivelu, R.; Nagappan, R.; Pragasan, L.A.; Ponnusamy, V.K. Microwave-assisted green synthesis of multi-functional carbon quantum dots as efficient fluorescence sensor for ultra-trace level monitoring of ammonia in environmental water. *Environ. Res.* **2022**, *206*, 112589. [[CrossRef](#)]
17. Kanaparthi, S.; Singh, S.G. Solvent-free fabrication of a room temperature ammonia gas sensor by frictional deposition of a conducting polymer on paper. *Org. Electron.* **2019**, *68*, 108–112. [[CrossRef](#)]
18. Gao, R.; Ma, X.; Liu, L.; Gao, S.; Zhang, X.; Xu, Y.; Cheng, X.; Zhao, H.; Huo, L. In-situ deposition of POMA/ZnO nanorods array film by vapor phase polymerization for detection of trace ammonia in human exhaled breath at room temperature. *Anal. Chim. Acta* **2022**, *1199*, 339563. [[CrossRef](#)]
19. Gai, S.; Wang, B.; Wang, X.; Zhang, R.; Miao, S.; Wu, Y. Ultrafast NH<sub>3</sub> gas sensor based on phthalocyanine-optimized non-covalent hybrid of carbon nanotubes with pyrrole. *Sens. Actuators B Chem.* **2022**, *357*, 131352. [[CrossRef](#)]
20. Kuprikova, N.M.; Klyamer, D.D.; Sukhikh, A.S.; Krasnov, P.O.; Mrsic, I.; Basova, T.V. Fluorosubstituted lead phthalocyanines: Crystal structure, spectral and sensing properties. *Dye. Pigment.* **2020**, *173*, 107939. [[CrossRef](#)]
21. Klyamer, D.; Sukhikh, A.; Gromilov, S.; Krasnov, P.; Basova, T. Fluorinated metal phthalocyanines: Interplay between fluorination degree, films orientation, and ammonia sensing properties. *Sensors* **2018**, *18*, 2141. [[CrossRef](#)] [[PubMed](#)]
22. Valli, L. Phthalocyanine-based Langmuir-Blodgett films as chemical sensors. *Adv. Colloid Interface Sci.* **2005**, *116*, 13–44. [[CrossRef](#)] [[PubMed](#)]
23. Schöllhorn, B.; Germain, J.P.; Pauly, A.; Maleysson, C.; Blanc, J.P. Influence of peripheral electron-withdrawing substituents on the conductivity of zinc phthalocyanine in the presence of gases. Part 1: Reducing gases. *Thin Solid Film.* **1998**, *326*, 245–250. [[CrossRef](#)]
24. Brinkmann, H.; Kelting, C.; Makarov, S.; Tsaryova, O.; Schnurpfeil, G.; Wöhrle, D.; Schlettwein, D. Fluorinated phthalocyanines as molecular semiconductor thin films. *Phys. Status Solidi Appl. Mater. Sci.* **2008**, *205*, 409–420. [[CrossRef](#)]

25. Germain, J.P.; Pauly, A.; Maleysson, C.; Blanc, J.P.; Schöllhorn, B. Influence of peripheral electron-withdrawing substituents on the conductivity of zinc phthalocyanine in the presence of gases. Part 2: Oxidizing gases. *Thin Solid Film.* **1998**, *333*, 235–239. [[CrossRef](#)]
26. Hesse, K.; Schlettwein, D. Spectroelectrochemical investigations on the reduction of thin films of hexadecafluorophthalocyaninatozinc (F16PcZn). *J. Electroanal. Chem.* **1999**, *476*, 148–158. [[CrossRef](#)]
27. Shao, X.; Wang, S.; Li, X.; Su, Z.; Chen, Y.; Xiao, Y. Single component p-, ambipolar and n-type OTFTs based on fluorinated copper phthalocyanines. *Dye. Pigment.* **2016**, *132*, 378–386. [[CrossRef](#)]
28. Kuzumoto, Y.; Matsuyama, H.; Kitamura, M. Partially fluorinated copper phthalocyanine toward band engineering for high-efficiency organic photovoltaics. *Jpn. J. Appl. Phys.* **2014**, *53*, 01AB03. [[CrossRef](#)]
29. Bonegardt, D.; Klyamer, D.; Sukhikh, A.; Krasnov, P.; Popovetskiy, P.; Basova, T. Fluorination vs. Chlorination: Effect on the Sensor Response of Tetrasubstituted Zinc Phthalocyanine Films to Ammonia. *Chemosensors* **2021**, *9*, 137. [[CrossRef](#)]
30. Klyamer, D.; Bonegardt, D.; Krasnov, P.; Sukhikh, A.; Popovetskiy, P.; Khezami, K.; Durmuş, M.; Basova, T. Halogen-substituted zinc(II) phthalocyanines: Spectral properties and structure of thin films. *Thin Solid Film.* **2022**, *754*, 139301. [[CrossRef](#)]
31. Klyamer, D.D.; Sukhikh, A.S.; Gromilov, S.A.; Kruchinin, V.N.; Spesivtsev, E.V.; Hassan, A.K.; Basova, T.V. Influence of fluorosubstitution on the structure of zinc phthalocyanine thin films. *Macroheterocycles* **2018**, *11*, 304–311. [[CrossRef](#)]
32. Becke, A.D. Density-functional exchange-energy approximation with correct asymptotic behavior. *Phys. Rev. A* **1988**, *38*, 3098–3100. [[CrossRef](#)] [[PubMed](#)]
33. Perdew, J.P. Density-functional approximation for the correlation energy of the inhomogeneous electron gas. *Phys. Rev. B* **1986**, *33*, 8822–8824. [[CrossRef](#)] [[PubMed](#)]
34. Weigend, F.; Ahlrichs, R. Balanced basis sets of split valence, triple zeta valence and quadruple zeta valence quality for H to Rn: Design and assessment of accuracy. *Phys. Chem. Chem. Phys.* **2005**, *7*, 3297–3305. [[CrossRef](#)]
35. Grimme, S.; Ehrlich, S.; Goerigk, L. Effect of the damping function in dispersion corrected density functional theory. *J. Comput. Chem.* **2011**, *32*, 1456–1465. [[CrossRef](#)] [[PubMed](#)]
36. Grimme, S.; Antony, J.; Ehrlich, S.; Krieg, H. A consistent and accurate ab initio parametrization of density functional dispersion correction (DFT-D) for the 94 elements H-Pu. *J. Chem. Phys.* **2010**, *132*, 154104. [[CrossRef](#)]
37. Baerends, E.J.; Ellis, D.E.; Ros, P. Self-consistent molecular Hartree-Fock-Slater calculations I. The computational procedure. *Chem. Phys.* **1973**, *2*, 41–51. [[CrossRef](#)]
38. Dunlap, B.I.; Connolly, J.W.D.; Sabin, J.R. On some approximations in applications of  $X\alpha$  theory. *J. Chem. Phys.* **1979**, *71*, 3396–3402. [[CrossRef](#)]
39. Van Alsenoy, C. Ab initio calculations on large molecules: The multiplicative integral approximation. *J. Comput. Chem.* **1988**, *9*, 620–626. [[CrossRef](#)]
40. Kendall, R.A.; Früchtl, H.A. The impact of the resolution of the identity approximate integral method on modern ab initio algorithm development. *Theor. Chem. Acc.* **1997**, *97*, 158–163. [[CrossRef](#)]
41. Eichkorn, K.; Treutler, O.; Öhm, H.; Häser, M.; Ahlrichs, R. Auxiliary basis sets to approximate Coulomb potentials. *Chem. Phys. Lett.* **1995**, *242*, 652–660, Erratum in *Chem. Phys. Lett.* **1995**, *242*, 652–660. [[CrossRef](#)]
42. Eichkorn, K.; Weigend, F.; Treutler, O.; Ahlrichs, R. Auxiliary basis sets for main row atoms and transition metals and their use to approximate Coulomb potentials. *Theor. Chem. Acc.* **1997**, *97*, 119–124. [[CrossRef](#)]
43. Weigend, F. Accurate Coulomb-fitting basis sets for H to Rn. *Phys. Chem. Chem. Phys.* **2006**, *8*, 1057–1065. [[CrossRef](#)] [[PubMed](#)]
44. Neese, F. The ORCA program system. *Wiley Interdiscip. Rev. Comput. Mol. Sci.* **2012**, *2*, 73–78. [[CrossRef](#)]
45. Neese, F. Software update: The ORCA program system, version 4.0. *Wiley Interdiscip. Rev. Comput. Mol. Sci.* **2017**, *8*, 73–78. [[CrossRef](#)]
46. Bühl, M.; Kabrede, H. Geometries of transition-metal complexes from Density-Functional Theory. *J. Chem. Theory Comput.* **2006**, *2*, 1282–1290. [[CrossRef](#)]
47. Keith, T.A. *AIMAll*, version 19.10.12; TK Gristmill Software: Overland Park, KS, USA, 2019. Available online: [aim.tkgristmill.com](http://aim.tkgristmill.com) (accessed on 5 September 2022).
48. Bonegardt, D.; Klyamer, D.; Krasnov, P.; Sukhikh, A.; Basova, T. Effect of the position of fluorine substituents in tetrasubstituted metal phthalocyanines on their vibrational spectra. *J. Fluor. Chem.* **2021**, *246*, 109780. [[CrossRef](#)]
49. Boys, S.F.; Bernardi, F. The calculation of small molecular interactions by the differences of separate total energies. Some procedures with reduced errors. *Mol. Phys.* **1970**, *19*, 553–566. [[CrossRef](#)]
50. Simon, S.; Duran, M. How does basis set superposition error change the potential surfaces for hydrogen-bonded dimers? *J. Chem. Phys.* **1996**, *105*, 11024–11031. [[CrossRef](#)]
51. Dunning, T.H. Gaussian basis sets for use in correlated molecular calculations. I. The atoms boron through neon and hydrogen. *J. Chem. Phys.* **1989**, *90*, 1007–1023. [[CrossRef](#)]
52. Bader, R.F.W.; Essén, H. The characterization of atomic interactions. *J. Chem. Phys.* **1984**, *80*, 1943–1960. [[CrossRef](#)]
53. Bader, R.F.W. A quantum theory of molecular structure and its applications. *Chem. Rev.* **1991**, *91*, 893–928. [[CrossRef](#)]
54. Bader, R.F.W. *Atom in Molecules: A Quantum Theory*; Oxford University Press: Oxford, UK, 1994.
55. Sukhikh, A.; Bonegardt, D.; Klyamer, D.; Basova, T. Effect of non-peripheral fluorosubstitution on the structure of metal phthalocyanines and their films. *Dye. Pigment.* **2021**, *192*, 109442. [[CrossRef](#)]

56. Klyamer, D.D.; Sukhikh, A.S.; Trubin, S.V.; Gromilov, S.A.; Morozova, N.B.; Basova, T.V.; Hassan, A.K. Tetrafluorosubstituted Metal Phthalocyanines: Interplay between Saturated Vapor Pressure and Crystal Structure. *Cryst. Growth Des.* **2020**, *20*, 1016–1024. [[CrossRef](#)]
57. Wisitsoraat, A.; Tuantranont, A.; Comini, E.; Sberveglieri, G.; Wlodarski, W. Characterization of n-type and p-type semiconductor gas sensors based on NiOx doped TiO2 thin films. *Thin Solid Film.* **2009**, *517*, 2775–2780. [[CrossRef](#)]
58. Chia, L.S.; Hua Du, Y.; Palale, S.; See Lee, P. Interaction of Copper Phthalocyanine with Nitrogen Dioxide and Ammonia Investigation Using X-ray Absorption Spectroscopy and Chemiresistive Gas Measurements. *ACS Omega* **2019**, *4*, 10388–10395. [[CrossRef](#)]
59. Ivanova, V.; Klyamer, D.; Krasnov, P.; Kaya, E.N.; Kulu, I.; Tuncel Kostakoğlu, S.; Durmuş, M.; Basova, T. Hybrid materials based on pyrene-substituted metallo phthalocyanines as sensing layers for ammonia detection: Effect of the number of pyrene substituents. *Sens. Actuators B Chem.* **2023**, *375*, 132843. [[CrossRef](#)]
60. Bushmarinov, I.S.; Lyssenko, K.A.; Antipin, M.Y. Atomic energy in the “Atoms in Molecules” theory and its use for solving chemical problems. *Russ. Chem. Rev.* **2009**, *78*, 283–302. [[CrossRef](#)]
61. Bejaoui, A.; Guerin, J.; Aguir, K. Modeling of a p-type resistive gas sensor in the presence of a reducing gas. *Sens. Actuators B Chem.* **2013**, *181*, 340–347. [[CrossRef](#)]
62. Chen, Y.; Yuan, M.; Zhang, Y.; Wang, X.; Ke, F.; Wang, H. One-pot synthesis of tin oxide/reduced graphene oxide composite coated fabric for wearable ammonia sensor with fast response/recovery rate. *J. Alloy. Compds.* **2023**, *931*, 167585. [[CrossRef](#)]
63. Li, Q.; Xu, M.; Jiang, C.; Song, S.; Li, T.; Sun, M.; Chen, W.; Peng, H. Highly sensitive graphene-based ammonia sensor enhanced by electrophoretic deposition of MXene. *Carbon* **2023**, *202*, 561–570. [[CrossRef](#)]
64. Zhang, L.; Zhang, H.; Chen, C.; Hu, Z.; Wang, J. Preparation and mechanism of high-performance ammonia sensor based on tungsten oxide and zinc oxide composite at room temperature. *Curr. Appl. Phys.* **2023**, *45*, 30–36. [[CrossRef](#)]
65. Ridhi, R.; Gautam, S.; Saini, G.S.S.; Tripathi, S.K.; Rawat, J.S.; Jha, P. Study of the effect of orbital on interaction behaviour of SWCNT-metal phthalocyanines composites with ammonia gas. *Sens. Actuators B Chem.* **2021**, *337*, 129767. [[CrossRef](#)]